A-1

ANS Reprint

SAFETY/ENVIRONMENTAL ASPECTS

MODELING OF LITHIUM FIRES

M. S. TILLACK and M. S. KAZIMI
Massachusetts Institute of Technology, Department of Nuclear Engineering
Cambridge, Massachusetts 02139

Received December 31, 1980
Accepted for Publication September 21, 1981

A computer code, LITFIRE, has been written to simulate the effects of lithium fires in fusion reactor containments. Development of the models in the code is discussed. Results of a study based on small-scale tests of lithium fires indicate that the code is capable of reasonable predictions of the temperature of the lithium pool and the atmosphere. However, the effects of simultaneous reactions with oxygen and nitrogen are the major source of uncertainty.

INTRODUCTION

Breeding tritium is a common objective of the conceptual designs of fusion power plants operating on a deuterium-tritium fuel cycle. This gives rise to a difficult choice of the chemical form of the breeding medium. The design trade-offs involve such concerns as tritium recoverability, total tritium inventory, breeding ratio, pumping power, chemical compatibility, corrosion, handling, and safety. The breeder may also act as the blanket coolant, which involves similar trade-off considerations.

The good heat transfer characteristics, breeding potential, and low activation level of pure lithium metal make it attractive not only as a breeder, but as a primary coolant as well. The principal disadvantages of lithium lie in safety and handling concerns stemming from its chemical reactivity.

The history of conceptual power reactor designs has not shown a steady commitment to any single breeding material. Early designs, such as UWMAK-I (Ref. 1) and UWMAK-III (Ref. 2), took advantage of the beneficial properties of lithium by making it the primary coolant. Some of the more recent designs, such as NUWMAK (Ref. 3) and STARFIRE (Ref. 4), have abandoned pure lithium in favor of compounds and eutectics of lithium. It is possible that misgivings over these compounds will lead back to the use of pure lithium, provided that the safety and handling issues can be resolved.

A computer code, LITFIRE, has been developed as a tool to quantify the consequences of the reactions of lithium and its compounds such that a more informed choice can be made from the various candidate coolants and breeders. At this time, LITFIRE has been verified against small-scale experimental spills that were performed at Hanford Engineering Development Laboratory[5] (HEDL). These comparisons have stimulated improvements in the modeling and given a measure of experience in proper application of the code. The purpose of this paper is to present an overview of the basic assumptions of the code and the results of the verification study. More detailed discussion may be found in Refs. 6 and 7.

LITFIRE MODEL DESCRIPTION

Background

Considerable effort has been invested in the development of methods for analysis of sodium fires, as applied to liquid-metal fast breeder reactor safety analysis. Lithium, however, is different from sodium in that it reacts exothermically with nitrogen (see Table I). Temperature-dependent kinetics of the lithium-air reactions warrant proper accounting for the Li-O_2 and Li-N_2 reactions separately.

The LITFIRE code development was initiated through modification of the sodium fire code in SPOOLFIRE (Refs. 7 and 8). The principal model modifications to create LITFIRE were inclusion of (a) the rate limited lithium-nitrogen reactions, (b) a combustion region above the surface of the

TABLE I

Chemical Reactions

	Heat of Reaction at 298 K (kcal/mol of product)
Lithium	
$4Li + O_2 \rightarrow 2Li_2O$	-143
$2Li + O_2 \rightarrow Li_2O_2$	-152
$6Li + N_2 \rightarrow 2Li_3N$	-48
$2Li + 2H_2O \rightarrow 2LiOH(c) + H_2$	-48.7
Sodium	
$4Na + O_2 \rightarrow 2Na_2O$	-99
$2Na + O_2 \rightarrow Na_2O_2$	-121
$2Na + 2H_2O \rightarrow 2NaOH(c) + H_2$	-44

liquid-metal pool, and (c) the effects of aerosol formation on the thermal properties of the atmosphere.

Basic Calculations

The LITFIRE code traces the movement of thermal energy from the source to the containment components and eventually out to the atmosphere. The atmosphere is approximated by a constant temperature infinite heat sink. The source term includes both the hot lithium metal and the fire, also called the combustion zone. In cases without lithium ignition, only the first term is present.

The one-cell version of LITFIRE is shown schematically in Fig. 1. The physical system is simulated by a nodal network in which each node has a heat capacity equal to that of its physical counterpart and an averaged corresponding temperature. Each node is assumed to be uniform in material composition and of constant thickness.

Properly estimated heat flows are calculated between any two nodes based, as appropriate, on the three heat transfer mechanisms—conduction, convection, and radiation. Exceptions occur when the effect of a particular heat transfer mechanism is negligible. For example, convection is the only heat transfer mechanism between the gas node and the extra heat capacity node, and conduction is the only mechanism between adjacent internal concrete nodes.

The heat flows mentioned above are computed using standard heat transfer relations. These are

$$\textit{convection} \qquad \dot{q} = h_c A (T_1 - T_2) \ , \tag{1}$$

$$\textit{conduction} \qquad \dot{q} = kA\frac{dT}{dx} \ , \tag{2}$$

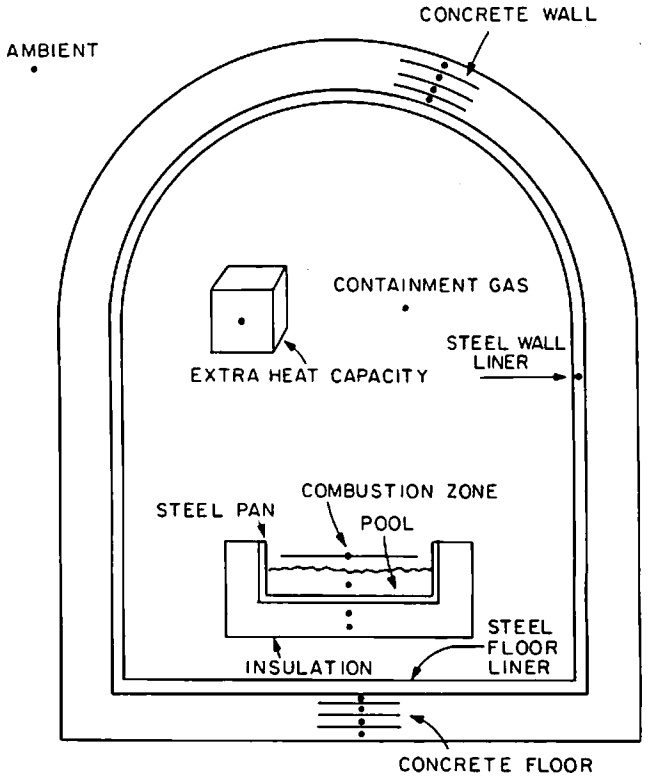

Fig. 1. One-cell node structure.

and

$$\textit{radiation} \qquad \dot{q} = \sigma AF(T_1^4 - T_2^4) \ . \tag{3}$$

(A Nomenclature appears on p. 244.) Determining the proper values for the coefficients h_c, k, and σF is fundamental to obtaining accurate results from LITFIRE.

In addition to heat flows, LITFIRE accounts for mass flows and chemical reaction rates. These include product formation in the pool, aerosol production and removal, cell leakage, lithium vapor diffusion to the combustion zone, and, most important, cell gas convection to the combustion zone (see Fig. 2). On the basis of observations made for sodium fires, one of the assumptions of LITFIRE is that the reaction rate is limited not by lithium vapor diffusion to the combustion zone, but by convection of reactive species in the cell gas to that zone.

The rate of mass convection is obtained by analogy to heat transfer. The heat transfer coefficient, h_c, is determined from

$$\mathrm{Nu} = c(\mathrm{GrPr})^{1/3} \ , \tag{4}$$

where

$$\mathrm{Nu} = h_c L/k \tag{4.a}$$

$$\mathrm{Gr} = g\beta\Delta T L^3/\nu^2 \tag{4.b}$$

$$c = \text{empirical constant} \ . \tag{4.c}$$

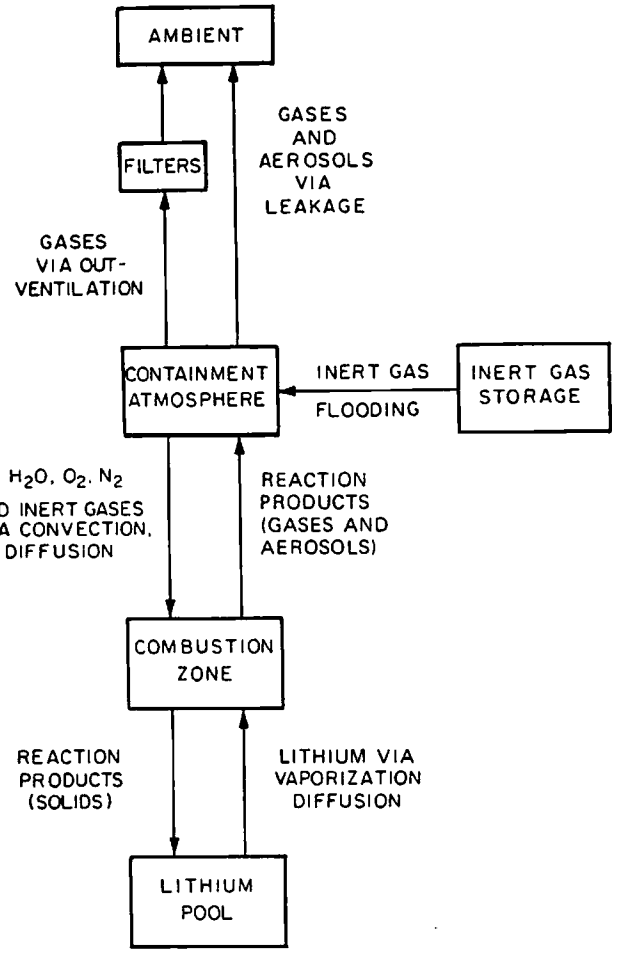

Fig. 2. Mass flow diagram for lithium pool combustion.

The mass transfer coefficient, h_m, is defined by

$$j_i = \rho h_m (w_{i,1} - w_{i,2}) \ , \tag{5}$$

where

j_i = mass flux of species i to the combustion zone

ρ = air density

$w_{i,1}$ = mass fraction of species i in bulk gas

$w_{i,2}$ = mass fraction of species i in the combustion zone region.

The coefficient h_m is computed using the correlation

$$\mathrm{Sh} = c(\mathrm{GrSc})^{1/3} \ , \tag{6}$$

where

$$\mathrm{Sh} = h_m L/D$$

$$\mathrm{Sc} = \nu/D \ . \tag{6.a}$$

Applying Reynold's analogy, setting the mass diffusivity equal to the thermal diffusivity, and assuming that Sc and Pr are approximately equal, it is easy to obtain

$$h_m = h_c/\rho C_p \ . \tag{7}$$

In the code, it is assumed that $w_{i,2}$ is negligibly small so that

$$j_i = \frac{h_c w_{i,1}}{C_p} \ . \tag{8}$$

An interesting consequence of the one-third power dependence in Eq. (4) is that h_c becomes independent of L, and, hence, the mass flux is independent of the size of the pool.

Unfortunately, the true reaction rate is much more complex and less understood than this simple model indicates. The effects of surface layer formation, wicking, bulk product buildup, multiple species competition, and suction due to gas consumption are all very difficult to accurately model. Yet improvement in these areas is critical, since the accuracy of the temperature profiles is limited to a large extent by the accuracy of the reaction rate.

Equation (4) is also used to determine the heat transfer by convection from all structures modeled in LITFIRE. The constant c is chosen in each case according to the shape, inclination, and position of the particular node. The value of L in Nu and Gr represents the characteristic linear dimension for that node.

To follow the containment response, LITFIRE solves a set of coupled equations describing the simultaneous processes of heat and mass transfer. It uses finite differences for the spatial dimensions, and either Simpson's Rule or a fourth-order Runge-Kutta integration in the time domain. Temperatures are computed at each time step for each node by integrating the energy balance equation as

$$mC_p \frac{dT}{dt} = \sum_i \dot{q}_i \ , \tag{9}$$

to obtain the integral equation

$$T(t) = T(t_0) + \int_{t_0}^{t} dt' \sum_i \frac{\dot{q}_i}{mC_p} \ . \tag{10}$$

The energy flows q_i are given for each node by finite difference solution of the heat transfer relations (1), (2), and (3). Masses are similarly computed from the mass flow rates.

LITFIRE Model Extensions

Two recent improvements have been incorporated[6] into LITFIRE. They are

1. a two-cell geometry allowing for the transfer of mass and energy between two adjacent cells

2. lithium-concrete combustion due to failure of the steel liner.

These are treated with a simple approach that accounts for the important processes taking place, as described below.

Two-Cell Code

There are at least two applications foreseen for the two-cell version of LITFIRE. It has been suggested that the reactor and blanket structure might be encapsulated in a small vessel separate from the steam generators and other components within the containment dome. This would constitute a mitigating influence on the potential combustion of lithium as well as an additional barrier to radiological release. If evacuated, the inner cell would aid in keeping the plasma clean during normal operation.

By limiting the amount of combustible gases available to the fire, the high temperatures and other destructive effects of an all-out fire may be eliminated. The two-cell code is able to analyze both the case of a fire contained within the inner cell, as well as the case of inner containment failure and subsequent mass and energy exchange with the outer cell.

The second application of the two-cell code is in analyzing the effects of pool burning within reactor components, for instance, inside pipes or even inside the plasma chamber. This calculation helps define the maximum temperatures to which irradiated structures may be subjected.

The configuration of the two-cell version of LITFIRE is shown schematically in Fig. 3. The inner cell has the same node structure as the one-cell code, except for the lack of a concrete wall and the presence of a break in the steel liner that allows for the exchange between cells. The outer cell is composed of nodes analogous to those in the inner cell, except for the lack of a lithium pool and the added presence of the concrete wall.

Both the leak rate between cells of the various gases and aerosols, as well as the effect of the leak on the primary and secondary cell gas node temperatures, are computed. The leak rate is calculated using an orifice relation,

$$\dot{m} = C_d A (2\rho \Delta p)^{1/2} , \qquad (11)$$

subject to the restriction that

$$\frac{P_{high}}{P_{low}} \leq \left(\frac{\gamma+1}{2}\right)^{\overline{\gamma/(\gamma-1)}} = 1.89 \text{ for air} . \qquad (12)$$

For larger pressure ratios than that of Eq. (12), the flow is choked and can be calculated independently of the downstream pressure. The cell gas temperatures are computed using the flow rate and a simple energy balance.

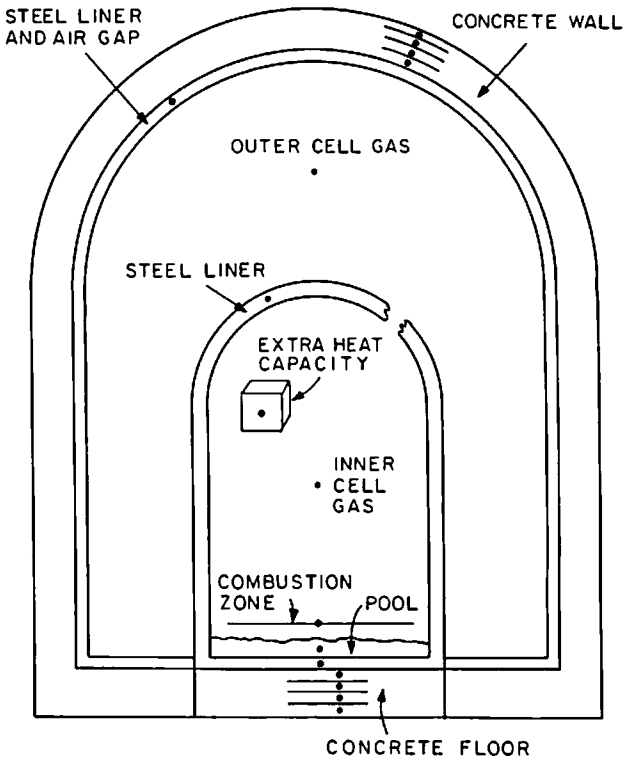

Fig. 3. Two-cell node structures.

Concrete Combustion

The amount of available chemical energy between lithium and concrete may be even more than for lithium-atmosphere reactions.[7] Thus, the possibility of contact between the concrete and lithium is a serious concern. In order to scope the possible effects of concrete combustion, a primitive model of this event has been included in the LITFIRE one-cell code.

The reactions occurring with the concrete have been studied at HEDL and by others. Some are listed in Table II. Rather than account for the details of the individual reactions, the model assumes that only one homogenized reaction occurs with an average heat of reaction equal to 150 kcal/mol lithium. This was calculated from HEDL data on the composition of the magnetite used in test LMC-1. In addition, the penetration rate of lithium through the concrete is taken to be a constant as determined from tests also performed at HEDL.

Water vapor combustion is handled separately. The reaction of concrete water with lithium takes place in the concrete combustion zone as rapidly as the water is released from the top concrete node. This release rate is obtained empirically from

TABLE II

Reactions of Lithium with Concrete

$$8Li + Fe_3O_4 \rightarrow 4Li_2O + 3Fe$$
$$4Li + SiO_2 \rightarrow 2Li_2O + 2Si$$
$$Li + H_2O \rightarrow LiOH + \tfrac{1}{2}H_2$$
$$2Li + H_2 \rightleftharpoons 2LiH$$
$$Li + LiOH \rightarrow Li_2O + \tfrac{1}{2}H_2$$
$$4Li + TiO_2 \rightarrow 2Li_2O + Ti$$
$$4Li + 3CO_2 \rightarrow 2Li_2CO_3 + C$$
$$6Li + Fe_2O_3 \rightarrow 3Li_2O + 2Fe$$

concrete heating experiments. Experimental data are scarce; further measurements are needed to improve this portion of the model.

Figure 4 contains a schematic representation of the concrete combustion zone node structure. Some of the assumptions made in modeling concrete combustion include:

1. The release of water vapor occurs from the top concrete node only. A restricted area of this node is defined for water vapor release; however, each concrete node still extends over the entire floor surface area.
2. The reaction zone never penetrates beyond the top concrete node.
3. The heat produced in the concrete combustion node leaves only by conduction to the lithium pool and concrete top node.
4. Except for hydrogen, the reaction products are confined to the concrete combustion zone node. The hydrogen is evolved to the cell gas.

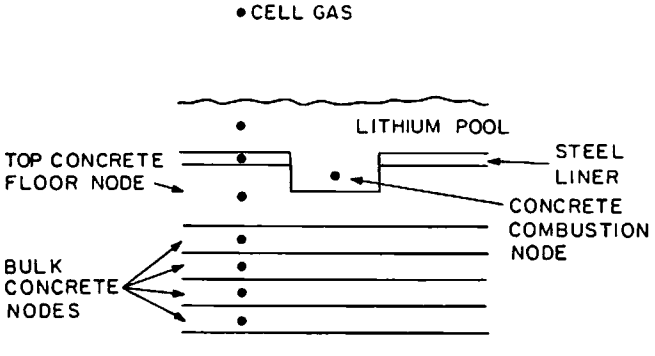

Fig. 4. Concrete combustion zone node structure.

Preliminary analysis of concrete combustion indicates that substantial evaporation of lithium is likely. Inclusion of this capability will be considered in future LITFIRE development.

DESCRIPTION OF LITHIUM SPILL EXPERIMENTS

The primary source of data for verifying the LITFIRE code is a series of small-scale lithium spills performed at the HEDL Large Sodium Fire Facility[5] (LSFF). Six different tests were performed by introducing 10 kg of preheated liquid lithium into atmospheres of carbon dioxide, pure nitrogen, and ordinary air. Table III summarizes the important parameters characterizing each test.

The verification of LITFIRE is based on measurements taken during each test, including temperatures, gas pressure, and spill pan weight. These values were monitored continuously for a 24-h period following the spills (although combustion was always completed in <4 h). In addition, discrete measurements were made during and after the tests to determine the composition of the aerosol, bulk gas, and reaction products remaining in the reaction pan. The diagram of the LSFF (see Fig. 5) gives detailed information on the location of the various components of the test cell and associated instrumentation.

After transferring the contents of the lithium holding tank into the spill pan, thermocouples monitored temperatures at various locations in the vessel for the remainder of the test. Five were placed in the center of the pool, supported by a vertical rod. Three were placed in contact with the spill pan, two in the bulk gas (one at 6 and one at 12 ft), and one thermocouple was placed in contact with the steel vessel 6 ft up. In addition, a pressure gauge at 5 ft measured the cell pressure, and a load cell kept track of the total mass of the reaction pan and its contents.

Post-test analysis of the spill pan and aerosol composition helped to identify which reactions had been present and how much aerosol was formed. In addition, grab samples taken during the tests were analyzed to determine the cell gas composition. These measurements provide a check on the estimate of the reaction rates as a function of time, temperature, and oxygen concentration. It is quite difficult to unravel the combined effects that drive the reaction rate unless a well-controlled experiment is designed for that specific purpose.

RESULTS

The tests performed at HEDL can be classified into three categories for the purpose of analysis and comparison. These are

TABLE III

HEDL Test Summary

	No Combustion		Single Species Combustion		Multiple Species Combustion	
	Test					
	LC-1	LN-1[a]	LN-2[a]	LN-3	LA-1	LA-2
Species in cell gas	CO_2	N_2	N_2	N_2	Normal air	Normal air
Initial lithium temperature, °C	238	222	532	840	243	519
Peak lithium temperature, °C[b]	238	224	534	916	1001	977
Initial gas temperature, °C	49	38	41	46	27	43
Peak gas temperature, °C	49	38	49	82	102	118

[a]Surface reaction observed.
[b]Or peak pan temperature when thermocouples failed.

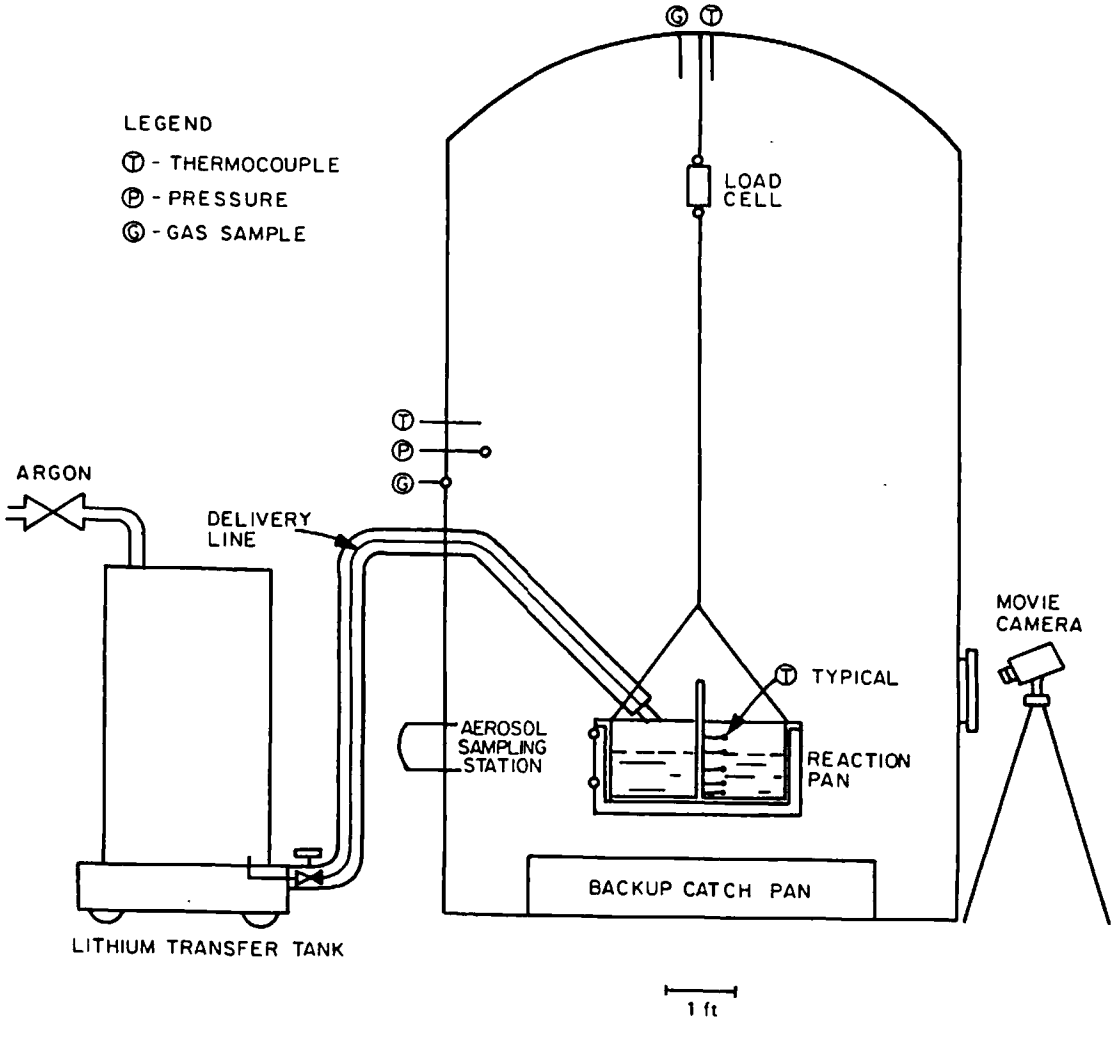

Fig. 5. HEDL test equipment arrangement.

1. tests that did not react to completion (LC-1, LN-1, and LN-2)
2. tests that reacted to completion in nitrogen only (LN-3)
3. tests that ignited in normal air and reacted to completion (LA-1 and LA-2).

This categorization is very helpful in separating out individual effects in determining the rate of heat transfer to cell gas and structures.

The results of experiments help in two distinct areas. First, differences between the predicted behavior and the experimental behavior motivated additions and changes to the model itself. Second, "best estimates" for the adjustable parameters in LITFIRE were obtained for these small-scale spills. In the following discussion, both aspects of the comparisons are described in some detail.

To define the containment response, critical areas in the structures and in the pool were examined including

1. cell gas temperature and pressure
2. steel vessel wall temperature
3. spill pan and/or lithium pool temperature.

Besides temperatures and pressures, a complete qualification of LITFIRE would have to include measurements of the reaction rates that form the source term. For LN-3, this was extracted directly from the pressure and temperature measurements. For LA-2, it was possible to compute the multiple species reaction rates using the HEDL oxygen concentration measurement. For LA-1, no reaction rate calculation was attempted due to lack of information on the pressure history at the time of analysis.

Tests with No Combustion

In tests with no active source term, the system simply responds passively to an initial disturbance away from thermal equilibrium. The predictions of LITFIRE are generally quite good for these tests (see Figs. 6 and 7). The lithium temperature profiles differ somewhat at early times in LN-1 and LN-2 due to an initial surface reaction that is eventually extinguished. The reaction dies because of the buildup of a protective product layer.

For nonignited runs, the parameters h_c, k, and σF in Eqs. (1), (2), and (3) are the most critical in determining the passive response of the containment. For the complicated geometry of a real reactor containment, the heat transfer coefficient and the radiative view factor will require qualitative judgment in selecting their values. Low temperature spills are dominated by convection, so naturally they were used to evaluate the proper selection

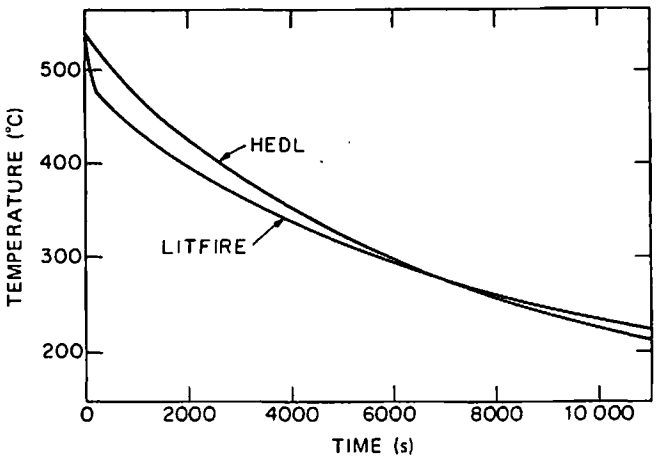

Fig. 6. LN-2 pool temperature.

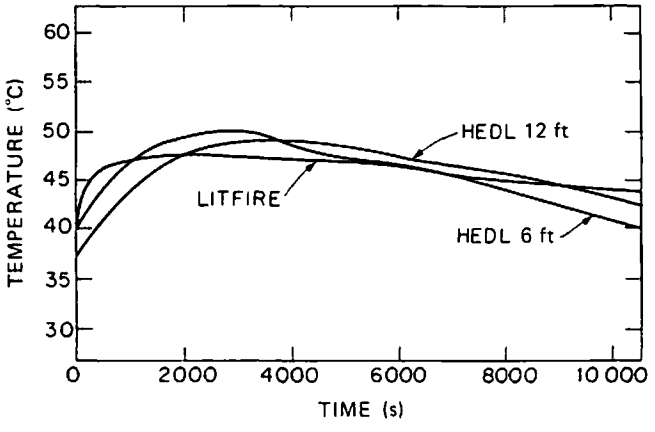

Fig. 7. LN-2 cell gas and steel vessel temperatures.

of the coefficient in the convection correlations, c, in Eq. (4). By making c a user-defined variable, the code can adapt to unusually shaped surfaces and the complicated enclosure effect. The following values for c were used:

Pool surface	0.12 ± 0.01
Vertical surface inside enclosure	0.11 ± 0.01
Vertical surface outside enclosure	0.07 ± 0.01
Oddly shaped components inside enclosure	0.09 ± 0.01 .

These values were obtained by trying to match all of the HEDL tests with a consistent set of coefficients.

There are several other processes modeled in LITFIRE that require user-selected input to the code. These "fine tuning knobs" allow flexibility

in treating various heat transfer parameters and when used properly will increase the accuracy of the code. They include the following.

1. *Dynamic properties*: The most important dynamic properties are cell gas and pool emissivities. The cell gas emissivity, ϵ_g, is computed using the quantity of aerosols released and a user-supplied mean aerosol surface area:

$$\epsilon_g = 1 - \exp(-xA_aL/4) \ , \qquad (13)$$

where

x = aerosol concentration, particle/m^3

A_a = aerosol particle surface area

L = optical path length to the walls.

The pool emissivity, ϵ_p, is computed from the equations

$$\epsilon_p = \epsilon_0 + (\epsilon_f - \epsilon_0)\frac{z}{z_f} \ , \quad z \leqslant z_f \qquad (14a)$$

and

$$\epsilon_p = \epsilon_f \ , \qquad z > z_f \ , \qquad (14b)$$

where

z = instantaneous product layer thickness

z_f = product layer thickness at which the pool emissivity has reached a maximum

ϵ_0 = initial pool thermal emissivity

ϵ_f = final pool thermal emissivity.

Suggested values for the input parameters are

$\epsilon_0 = 0.2$

$\epsilon_f = 0.9$

$z_f = 2.0$ mm .

2. *Radiative view factors*: Currently, the view factors are computed for the user based on the node surface areas input to the code.[6-8]

3. *Transient natural convection*: Since the entire cell gas volume is modeled by a single node, a time constant is incorporated into the calculation of heat and mass transfer coefficients from the pool. This time constant delays the response of the cell gas temperature, particularly during the initial phase of the fire. Torrance and Rockett[9] suggest that the time constant, τ, is related to the Grashof number by

$$\tau = \frac{12L^2}{\alpha}\mathrm{Gr}^{-1/2} \ , \qquad (15)$$

where α is the thermal diffusivity of air, L is the containment height, and the properties are evaluated at the bulk gas temperature. Thus, the heat transfer coefficient at any time step, h, is related to the heat transfer coefficient at the preceding step, h_0, by

$$h = h_f + (h_0 - h_f)\exp(-\Delta t/\tau) \ , \qquad (16)$$

where h_f is the asymptotic coefficient defined by the steady-state Eq. (4).

Tests with Nitrogen Combustion Only

When combustion is taking place, the emphasis shifts to the so-called combustion zone, shown schematically in Fig. 8. The principal mode for heat transfer in high temperature ignited runs is radiation rather than convection. This case is therefore more useful in defining the dynamics of the combustion zone as well as the response of the containment to radiation heat transfer. Analysis of the LN-3 test has helped to improve both the energy flows near the combustion zone and the mass flows, which determine the reaction rate.

Temperature Dependence of Nitrogen Reaction Rate

The dependence of the nitrogen reaction rate on temperature reflects the assumption that combustion is suppressed below the melting point of lithium (225°C) or above 1025°C where Gibb's free energy implies a preferred reversed direction for the reaction between lithium and nitrogen (Fig. 9). This is illustrated in Fig. 10, where the peak in the curve is fixed by assuming that at some point there is no hindrance, and all available nitrogen combines as fast as it can reach the combustion zone. The observations from LN-2 and LN-3 suggested that the parabolic form originally assumed needed to be altered to the new shape as shown in Fig. 10. This shape is still crude and should be further refined in the future, as more experiments become available.

The absence of complete reaction for LN-2 at a pool temperature of 530°C led to reducing the reaction rate at that temperature such that convection and radiation cooled the pool faster

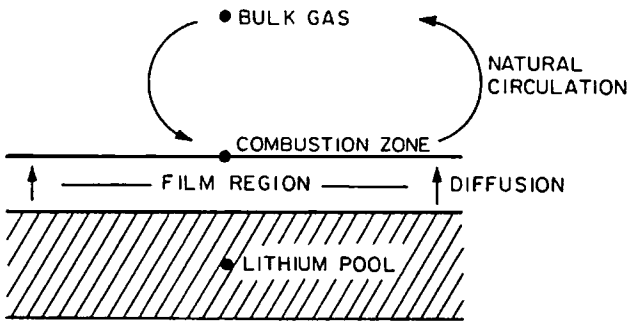

Fig. 8. Combustion zone geometry.

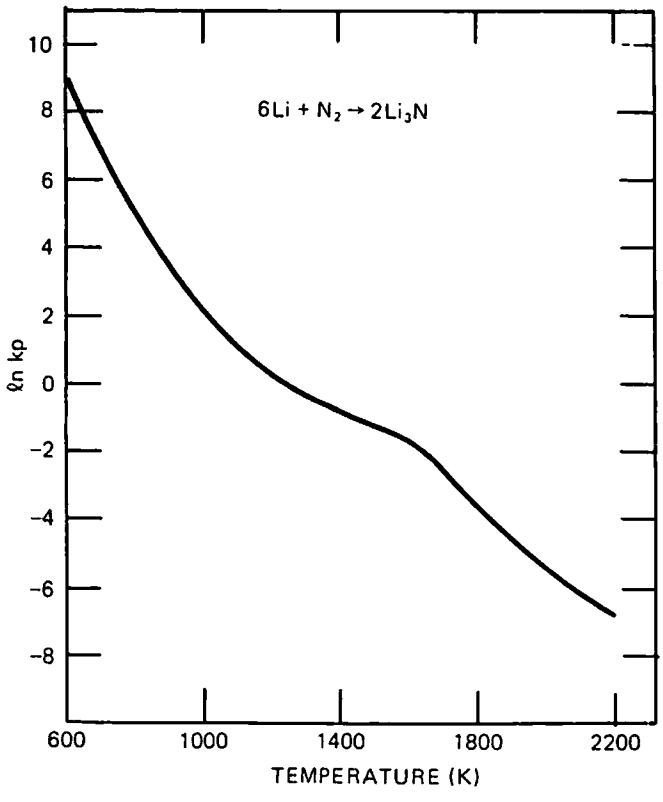

Fig. 9. Li_3N equilibrium constant.

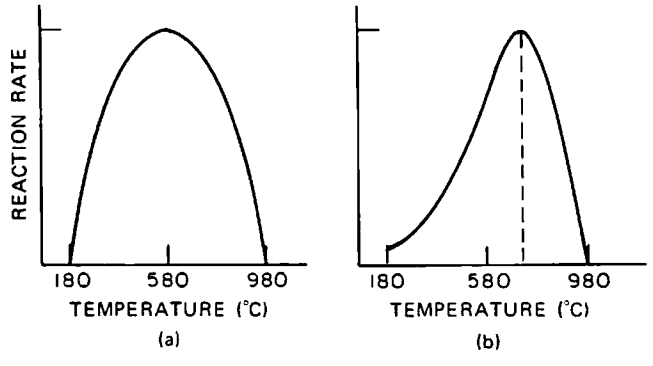

Fig. 10. Nitrogen reaction rate curves: (a) previous form and (b) current form.

than combustion heated it. On the other end, rapid combustion near the thermochemical cutoff during LN-3 suggested that the entire curve should be pushed up in temperature. However, the new curve generated by these two operations is not uniquely defined by the limited available data.

In addition, the appropriate reference temperature for evaluation of the reaction rate must be defined. Currently, LITFIRE uses a single value of temperature equal to the average of the combustion zone and pool temperatures. A more detailed account of the temperature variation between the pool surface and the combustion zone may provide improved values of the reaction rate.

Mass Transport to the Combustion Zone

Based on the experimental observation of violent churning in the pool as well as the fact that gases are being consumed in the combustion zone, one might expect more turbulence in that region and, therefore, more heat and mass transfer. In addition, the vacuum left when nitrogen is solidified into Li_3N is a driving term not previously considered in the LITFIRE model. This turbulence and suction effect could explain the initial speed of reaction not predicted by our model. As seen in Fig. 11, after 1500 s the actual rate falls below the prediction, presumably due to product formation.

Independent tests on nitrogen-lithium combustion confirm both the initial enhancement and the later inhibition of the reaction rate.[10] A theory has been postulated by Ostroushka et al.,[11] which expresses the extent of the reaction, α, as

$$\alpha = 1 - \exp(-kt^n) \quad , \qquad (17)$$

where k and n are undetermined parameters. This formulation has not yet been applied to experimental comparisons.

Combustion Zone, Film, and Cell Gas Properties

In the early comparisons, it became clear that the model underpredicted the lithium pool temperatures. The problem was identified as poor coupling between the combustion zone and the pool—too much heat was being sent up to the cell gas and steel vessel, and too little to the pool. A review of the assumptions in the original model led to three alterations that resulted in better agreement with the experiments. These alterations are

1. The composition of the film region was changed from pure nitrogen to a mixture of nitrogen and lithium vapor. The thermal conductivity is then obtained from a pressure-weighted average of both vapors. This gives roughly the same order of conductivity in the high temperature range (above 1200°C), but a sizable enhancement at lower temperature (typical peak pool temperatures are ~1000°C). Unlike most vapors, lithium shows an increase in thermal conductivity as the temperature decreases.

2. The thermal emissivity of the combustion zone was reduced from 0.5 to 0.1. The previous assumption that the flames are luminous and therefore are opaque grey bodies is based on the existence of macroscopic product aerosols that effectively block the line of sight from the pool. However, if one assumes that the combustion zone is extremely

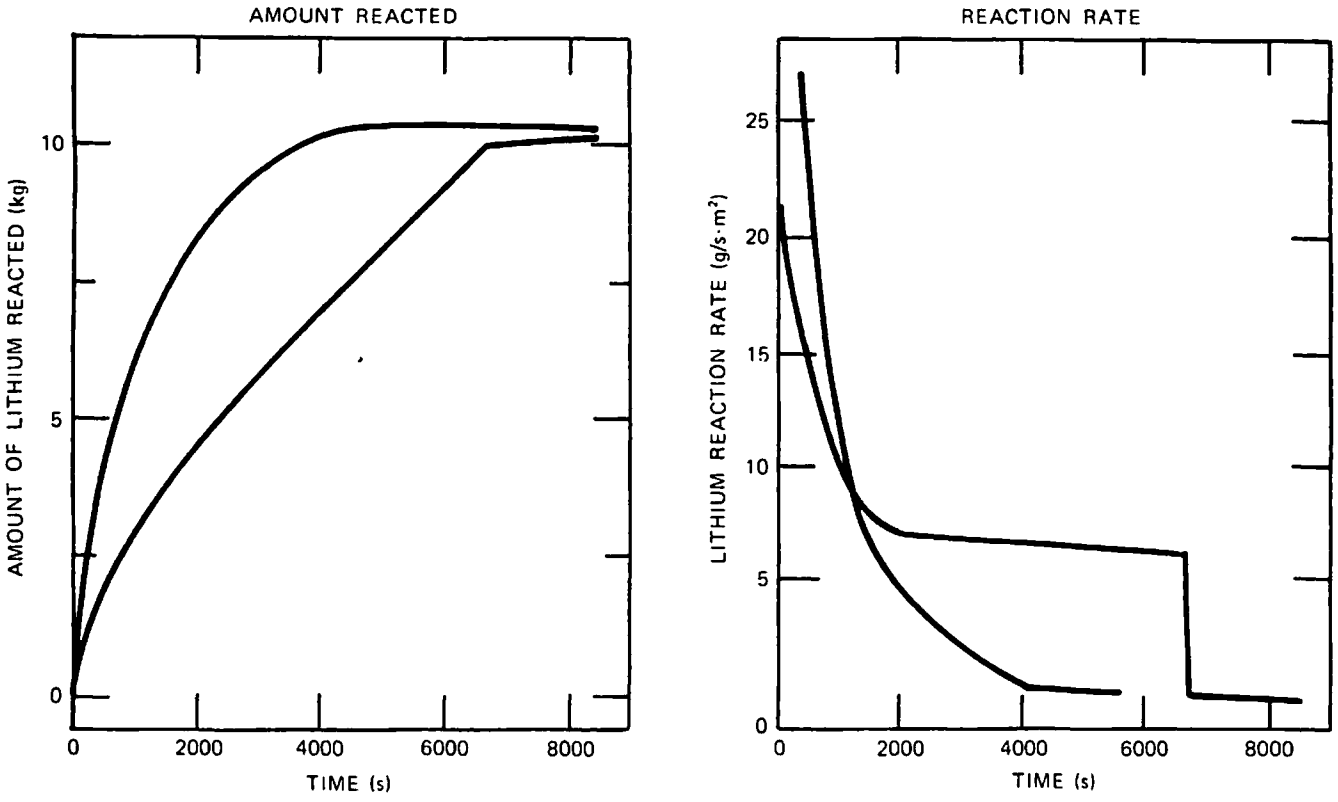

Fig. 11. LN-3 lithium consumption curves.

thin, as the model does, then luminescence does not necessarily follow.

Like most vapors, lithium emits primarily at its discrete rotational/vibrational lines, most of which lie between 8708 and 2302 Å. Away from these lines, the vapor is essentially transparent. Ignoring for the moment the reaction products, if the combustion zone emits only at characteristic lines, then the pool should be strongly absorbing at those same lines. This implies that the combustion zone should radiatively couple well with the pool, but not necessarily with the gas. In fact, the narrow range of frequencies that is excited should lead to a fairly low-averaged emissivity.

3. The gas emissivity was kept below 0.05. Since the cell gas temperature is one of the most important parameters, it is necessary to develop a reasonably accurate model to predict the dynamics of aerosol generation and removal. In the past, the model would allow the release of a fraction of the combustion products into aerosol, but include no mechanism for removal.

With no mechanism for aerosol removal, the ultimate gas emissivity is always 1.0 provided there is enough product evolved. This state is reached very quickly (at ~100 s) when as little as 5% of the product is released. In reality, a balance between production, agglomeration, and removal may conceivably lead to lower ultimate emissivities.

Multiple Species Combustion

Because tests with normal air are ignited runs, the emphasis is still on the combustion zone and radiation heat transfer. The most notable feature over the LN-3 results is multiple species combustion kinetics. As observed at HEDL, the smoke generated during lithium-air combustion is mostly Li_2O, some LiOH, and virtually no Li_3N. Therefore, unlike nitrogen tests, the gas emissivity changes a great deal throughout the fire.

The effect of oxygen concentration on the nitrogen combustion rate must be included as well as the effects of temperature and of nitrogen concentration on the oxygen combustion rate. These simultaneous effects make it extremely difficult to infer precise relationships from the limited sample of experimental data.

To investigate the accuracy with which LITFIRE predicts combustion rates, the ideal gas law

$$PV = nRT \tag{18}$$

was applied to the profiles of temperature and pressure. The results shown in Fig. 12 indicate that gas consumption rates are substantially lower

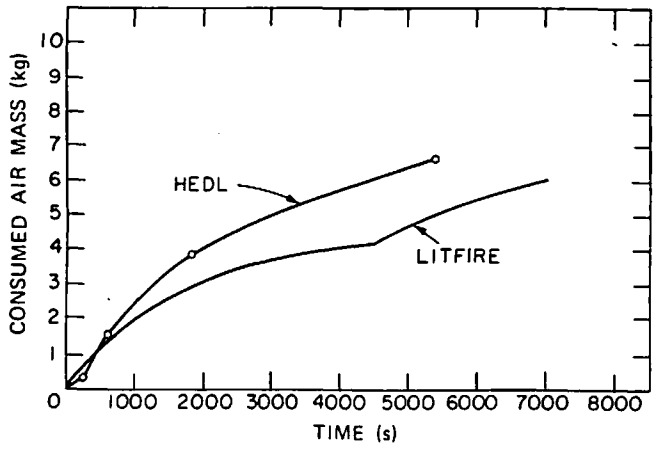

Fig. 12. Amount of gases consumed during test LA-2.

in the LITFIRE prediction. The reason for this underprediction could stem from the gas diffusion model or from the assumed temperature and oxygen concentration dependence of the nitrogen reaction rate. The comparison shown in Fig. 13 for the oxygen concentration profiles tends to support this latter conclusion. The higher values of oxygen concentration measured experimentally imply that in LITFIRE nitrogen is not being consumed fast enough in relation to oxygen.

There are two potential explanations for this effect. Both depend on an accurate definition of the temperature and oxygen concentration at the exact location where reactants combine. Since oxygen is not hindered from reacting the way nitrogen is, it can be presumed that the combustion zone is an oxygen-poor environment compared to the bulk gas. In calculating the nitrogen reaction rate versus oxygen concentration, since we use the bulk values of O_2 and N_2 masses, we should expect to be overpredicting the oxygen concentration. This leads directly to lower values of the nitrogen reaction rate.

The other possible explanation involves the large temperature gradient that exists between the combustion zone and cell gas, and also between the combustion zone and pool. If some combustion occurs outside the boundary of our idealized, infinitely thin combustion zone node, then the true temperature at the reaction site is not nearly as high as predicted. Because of the steep dependence of the nitrogen reaction rate on temperature, even small temperature gradients could be very important.

CONCLUSIONS

The limited verification study of LITFIRE as applied to HEDL data leads to the following conclusions.

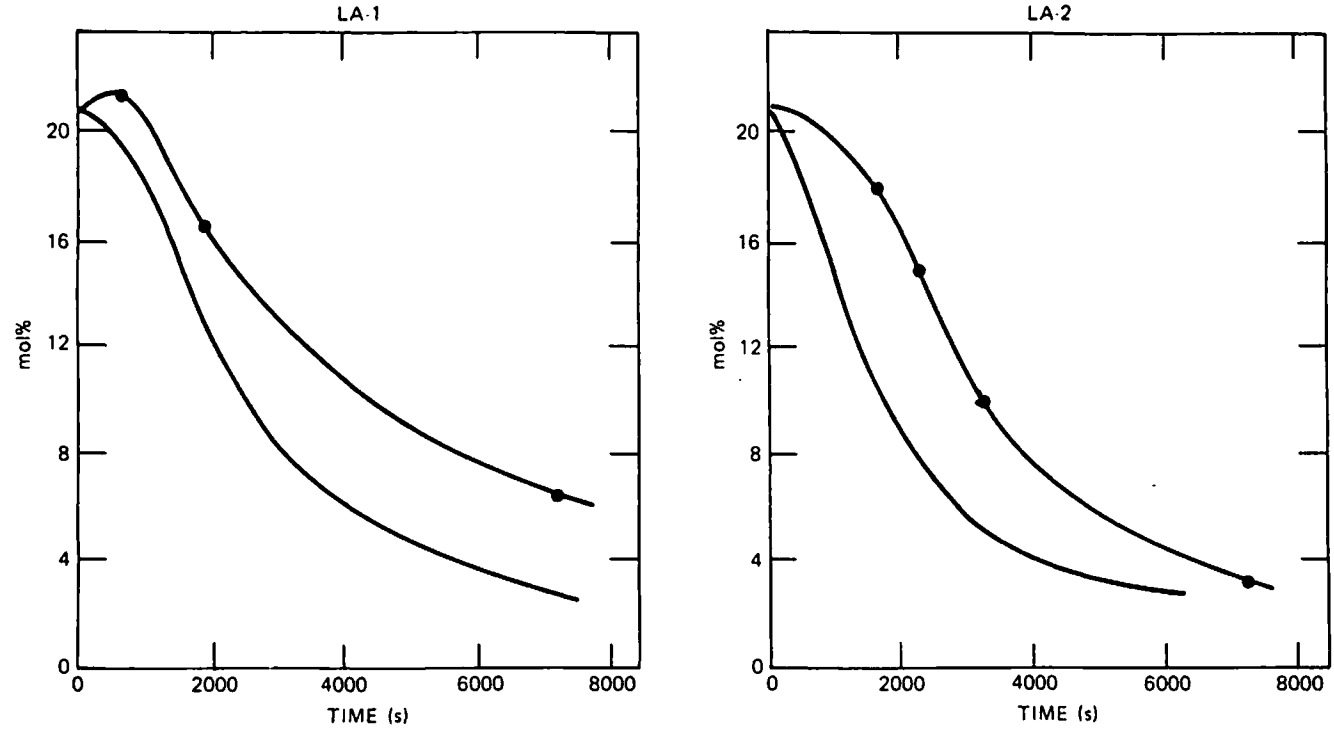

Fig. 13. LA-1 and LA-2 oxygen concentration history.

1. As simplified as the model of LITFIRE is, it has been successful in predicting thermal response of the test cell in the cases of a lithium spill without fire as well as the single-species fire in nitrogen atmospheres.
2. The multiple species fires are not as well predicted by LITFIRE as desirable. The complications arising from both the interdiffusion of the gases and the temperature dependence of the reaction rates will require more experimental data to be properly evaluated.
3. For the gas emissivity to be well predicted, the effect of aerosol production and removal to the gas must be investigated. This area is particularly significant for oxygen fires where the aerosol generation has been experimentally observed. The nitrogen fires were properly modeled without aerosol formation effects.
4. Several features of the lithium fire model need to be evaluated further. These are summarized in Table IV. It is also important to conduct tests of lithium fires in volumes larger than the tests conducted to date to ensure the adequacy of size scaling of the present model parameters.

NOMENCLATURE

A = surface area

C_d = coefficient of discharge for orifice

C_p = specific heat

D = mass diffusivity

F = radiation view factor, including emissivity

g = acceleration of gravity

h_c = coefficient of heat transfer by convection

h_m = coefficient of mass transfer by convection

j = mass flux

k = thermal conductivity

L = linear dimension

m = mass

$\dot{m}$ = mass flow rate

p = gas pressure

$\dot{q}$ = heat flow rate

T = temperature

w_i = mass concentration of species i

β = coefficient of volume expansion

γ = c_p/c_v

ϵ = thermal emissivity

ν = kinematic viscosity

ρ = gas density

σ = Stefan-Boltzmann constant

TABLE IV

Summary of Areas for Further Development in Lithium Reaction Modeling

1. Improvements to Reaction Rate Calculations
   a. temperature dependence for nitrogen combustion
   b. evaluation of proper reference temperature
   c. mass transport effects, suction and turbulence
   d. product buildup
   e. multiple species effects (nitrogen reaction rate hindrance versus oxygen concentration)
2. Properties
   a. combustion zone emissivity and transmissivity
   b. gas emissivity
3. Concrete Combustion
   a. accurate water release rates from heated concrete
   b. inclusion of lithium evaporation capability

REFERENCES

1. "UWMAK-I, A Wisconsin Toroidal Fusion Reactor Design," UWFDM-68, Fusion Feasibility Study Group, University of Wisconsin (Mar. 15, 1974).

2. "UWMAK-III, A Non-Circular Tokamak Power Reactor Design," UWFDM-150, Fusion Feasibility Study Group, University of Wisconsin (July 1976).

3. "NUMAK," UWFDM-330, Fusion Feasibility Study Group, University of Wisconsin (Mar. 1979).

4. C. C. BAKER et al., "STARFIRE, A Commercial Tokamak Fusion Power Plant Study," ANL/FPP-80-1, Argonne National Laboratory (Sep. 1980).

5. D. W. JEPPSON, "Interactions of Liquid Lithium with Various Atmospheres, Concretes, and Insulating Materials; and Filtration of Lithium Aerosols," HEDL-TME-79-7-UC-20, Hanford Engineering and Development Laboratory (June 1979).

6. M. S. TILLACK and M. S. KAZIMI, "Development and Verification of the LITFIRE Model for Predicting the Effects of Lithium Spills in Fusion Reactor Containments," PFC/RR-80-11 (July 1980).

7. D. A. DUBE and M. S. KAZIMI, "Analysis of Design Strategies for Mitigating the Consequences of Lithium Fire

Within Containment of Controlled Thermonuclear Reactors," MITNE-219, Massachusetts Institute of Technology (July 1978).

8. I. CHARAK and L. W. PEARSON, "SPOOLFIRE: Analysis of Spray and Pool Na Fire," presented at the American Nuclear Society Mtg. on Fast Reactor Safety and Related Physics, Chicago, Illinois, October 1976.

9. K. E. TORRANCE and J. A. ROCKETT, "Numerical Study of Natural Convection in an Enclosure with Localized Heating from Below-Creeping Flow to the Onset of Laminar Instability," *J. Fluid Mechanics*, **36**, 1 (1969).

10. E. W. JEPPSON et al., "Lithium Literature Review: Lithium's Properties and Interactions," HEDL-TME-78-15, Hanford Engineering and Development Laboratory (Apr. 1978).

11. S. OSTROUSHKA et al., "Lithium, Its Chemistry and Technology," AEC-RR-4940, U.S. Atomic Energy Commission (1960).